FINAL REPORT

EVALUATION OF NONDESTRUCTIVE EVALUATION METHODS FOR APPLICATION IN EARLY DETECTION OF DETERIORATION IN CONCRETE PAVEMENTS

Gerardo G. Clemeña, Ph.D.
Principal Research Scientist

D. Stephen Lane
Senior Research Scientist

Thomas E. Freeman, P.E.
Senior Research Scientist

Margarit G. Lozev, Ph.D.
Senior Research Scientist

(The opinions, findings, and conclusions expressed in this
report are those of the authors and not necessarily
those of the sponsoring agencies.)

ABSTRACT

Three nondestructive evaluation (NDE) methods for concrete pavements—surface ultrasonic pulse velocity measurements (UPV), the impact-echo (IE) method, and the use of a seismic pavement analyzer (SPA)—were tested on six sections of two continuously reinforced concrete pavements. The results were compared with the actual condition of the concrete as determined by visual inspection, photographic imaging, and examination of cores extracted from the sections.

The IE and surface UPV methods were the best in indicating the existence of macroscopic cracks. However, each must be used over a relatively long period of time to determine the deterioration rate of pavement. In addition, to be practical and efficient for application in pavement inspection, mechanization of the instrumentation of each method would be required.

Even though the SPA did not compare favorably with the IE and surface UPV methods in detecting cracks and delaminations, it provided information that could be used to derive the overall qualitative condition of each test section. The results with the SPA had a high correlation with a petrographically determined rating for alkali-silica reactivity. This correlation, if verified, can serve as the basis for using the inspection system to collect information that may be used to predict the future condition of a pavement. In addition, the SPA is already associated with a hardware/software system. In comparison with the other methods, the SPA would require the least additional development in its hardware/software system to be an effective rapid inspection system.

Photographic imaging was extremely valuable. Although it did not probe into the concrete as did the three NDE methods/systems investigated, it captured the surface cracks and other surface features that may well be useful indicators of the future condition of the pavements. In view of the recent advancements in the technology of high-resolution digital imaging systems and computers that can make this inspection method quantitative, which it seriously needs to be, photographic imaging deserves attention as an NDE method.

FINAL REPORT

EVALUATION OF NONDESTRUCTIVE EVALUATION METHODS FOR APPLICATION IN EARLY DETECTION OF DETERIORATION IN CONCRETE PAVEMENTS

Gerardo G. Clemeña, Ph.D.
Principal Research Scientist

D. Stephen Lane
Senior Research Scientist

Thomas E. Freeman, P.E.
Senior Research Scientist

Margarit G. Lozev, Ph.D.
Senior Research Scientist

INTRODUCTION

Many sections of continuously reinforced concrete pavement on I-295 near Richmond, Virginia, were built in the 1980s and have shown signs of progressive deterioration. The most significant patterns of distress are potholes, cracking, and punch outs at closely spaced transverse cracks; map cracking (with a strong longitudinal trend); and delamination of the slab at the level of the steel. The major mechanisms that have been associated with these patterns of distress are excessive shrinkage and alkali-silica reactivity (ASR) in the concrete, corrosion of steel bars, and poor drainage. It is suspected that many newer sections of continuously reinforced concrete pavement in other areas will likely suffer similar deterioration in the future. Because of the high cost of rehabilitating damaged concrete pavements, this situation presents a major challenge to pavement maintenance engineers to develop an effective maintenance strategy. However, the development of such a strategy requires the ability to detect and quantify the various types of distress at an early stage—preferably before they become apparent—when the repair would likely be less expensive. Unfortunately, there is no proven inspection method available for this purpose, and previous attempts to detect this type of damage by sounding concrete (with chain-drags and other similar tools) have not been successful.

PURPOSE AND SCOPE

The objective of this investigation was to identify NDE methods that can indicate forthcoming problems in a continuously reinforced concrete pavement with a reasonable degree of reliability. This required testing pavement sections with visible signs of distress representative

of various stages of severity not only among test sections but also among different areas or locations within a test section.

EXPERIMENTAL APPROACH

The investigation essentially involved (1) selecting representative test sections of concrete pavements with transverse and map cracking in various stages of severity, (2) selecting candidate NDE methods for evaluation, (3) using each method on all test sections, and (4) assessing the relevancy of the information provided by each method with regard to the condition of the test sections.

Test Sections

Six test sections were selected (Table 1). Within each test section, several longitudinal test locations 0.60 by 0.90 m were used to test the NDE methods, providing a total of 47 test locations. The pavement cross sections at these sites were similar and consisted of a concrete slab 200 mm thick, longitudinally reinforced with steel bars at about 130 mm below the surface, over a base 150 mm thick (stabilized with either cement or asphalt), over a soil subgrade. The concrete slabs in three of the sections (1, 3, and 5) had closely spaced transverse cracks at many locations (Figure 1), and those in the other sections (2, 6, and 7) had fine longitudinal cracks and "wet" streaks (Figure 2). Test section 4 was deleted from the study because it was deemed that these six sites would suffice

Table 1. Test Sections

Test Section	Roadway	Location	No. of Locations	Prevalent Pavement Distress
1	I-295	Eastbound lane near Exit 53	8	Transverse cracks, delaminations
2	I-295	Eastbound lane (slow) east of MP 43	10	Longitudinal cracks, delaminations, ASR
3	I-295	Eastbound lane (slow) south of MP 29	6	Transverse cracks, delaminations
5	Rt. 60	Westbound land (slow) east of Exit 28 from Rt. 295	8	Transverse cracks, delaminations
6	I-295	Eastbound lane (slow) before Exit 37	8	Longitudinal cracks, delaminations, ASR
7	I-295	Eastbound lane (fast) before Exit 34	7	Longitudinal cracks, delaminations, ASR
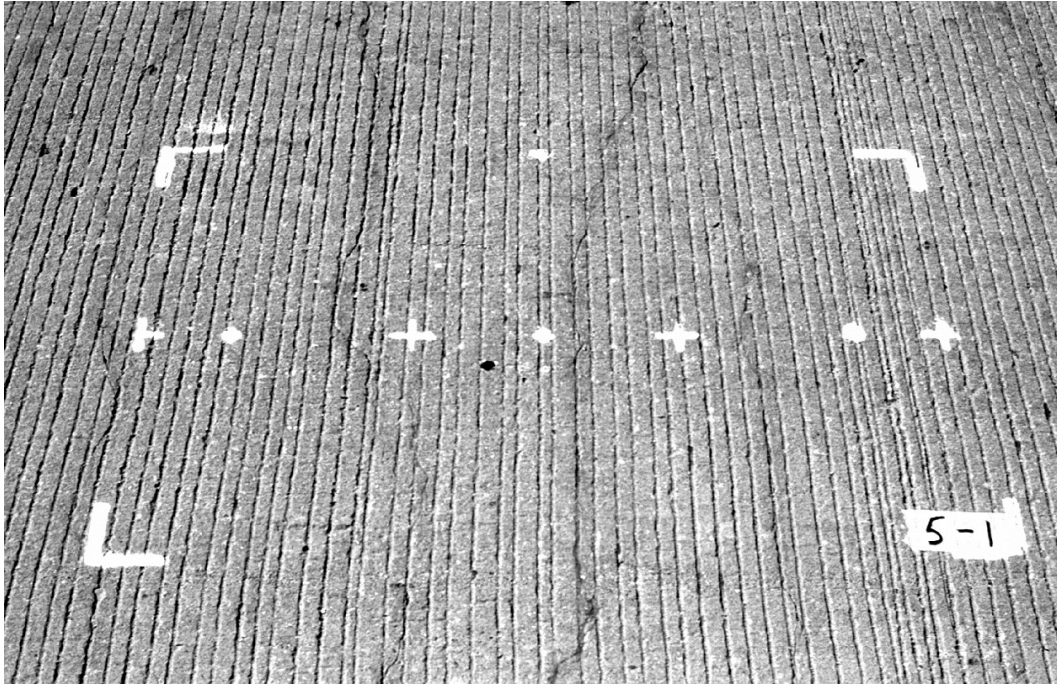
Figure 1. Test location 5-1 with transverse cracks. The corresponding scale and significance of the various paint markings are provided in Figure 4.
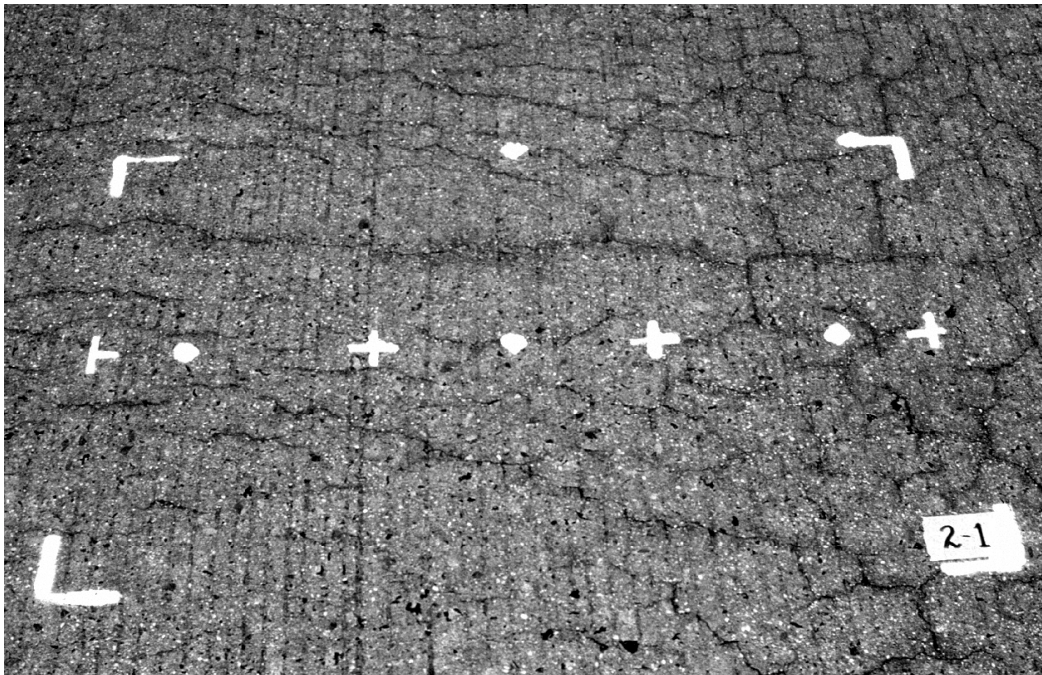
Figure 2. Test location 2-1 showing longitudinal and map cracking.

3
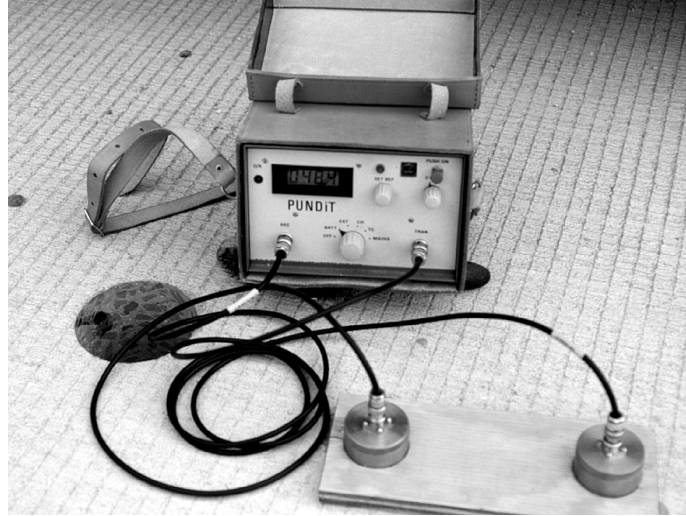
Figure 3. UPV meter.

NDE Methods

The three NDE methods selected for evaluation were the surface measurement of ultrasonic pulse velocity (UPV), the impact-echo (IE) method, and the use of the seismic pavement analyzer (SPA). These methods were selected because all involved the use of elastic and/or sonic wave propagation, which is quite sensitive to the presence of defects in solid materials such as concrete. Further, these methods either may be already sufficiently developed or have the potential to be developed for NDE of continuously reinforced concrete pavement.

Surface Measurement of UPV

This nondestructive method was selected because it allows measurement of the velocity (v_c) of a compression (longitudinal) wave through a material by measurement of the transit time (t) of a compression wave travelling across the material of known thickness (d). And, as the following expression indicates, if the Poisson's ratio (μ) and density (ρ) of the material are known, this property, in turn, allows the determination of the modulus of elasticity (E), which is a measure of its quality.[1]

$$v_c = \frac{d}{t} = \sqrt{\frac{(1-\mu)gE}{(1+\mu)(1-2\mu)\rho}} \qquad \text{[Eq. 1]}$$

Other desirable aspects of this method are that it is simple to perform and requires only a relatively inexpensive instrument that is commercially available. However, if UPV measurements are found to be useful for NDE of concrete, a mechanized version of the necessary instrumentation will need to be developed for it to be practical for pavements.

UPV measurements are made by one of three possible methods (direct transmission, semi-indirect transmission, and indirect or surface transmission), depending on the accessibility of the objects being evaluated or inspected. Among these, the direct or through transmission method, whereby an ultrasonic transmitter is attached to one side and a receiver is attached directly to the opposite side of the test object, provides the best sensitivity and is, therefore, the most preferable. In fact, Bungey used this method to observe a reduction in UPV in concrete specimens affected by ASR.[2] Unfortunately, this method cannot be used in testing concrete pavements, where only the surface of the concrete slab is accessible to any type of probe or transducer. The semi-indirect transmission method is used specifically for corners of test objects, where the two transducers are placed on opposite sides of a corner, and was not applicable for this situation. This left only the surface transmission method, whereby both transducers are coupled to one side or the surface, for possible use in of pavement inspection.

Impact-Echo Method

IE is also based on the propagation of stress waves in the concrete member being tested.[3] A probing transient stress pulse is introduced into the concrete slab by mechanically impacting its surface with a spherical steel ball (of a size appropriate for the thickness of the slab). The reflections of this stress pulse from the boundaries of the slab and cracks or defects in the concrete are picked up by a piezoelectric transducer coupled to the surface of the concrete and then analyzed to determine their depth (d), assuming a certain compression wave speed. If there is no defect in the concrete slab or its thickness (d) is known (within a reasonable precision), the compression wave speed (v_c) of the concrete can be determined to provide an indication of the quality of the concrete through comparison with another concrete of known quality; that is:

$$v_c = 2fd$$ [Eq. 2]

where f is the resonance frequency corresponding to the reflections.

Seismic Pavement Analyzer

The use of a combination of several NDE techniques, including IE, impulse response, ultrasonic surface waves, and ultrasonic compression waves, to comprise an inspection system is made possible by the recently developed SPA.[4] This system uses high- and low-frequency pneumatic hammers to introduce interrogating waves into the pavement and four accelerometers and two geophones to sense the responses of the pavement to the waves. From the responses of a pavement and the arrival times of various direct and refracted waves, the system provides estimates of the thickness of the paving layer, or depth of a delamination in the paving layer, Young's and shear moduli of the top paving layer, etc., using Eq. 2 and the following additional expressions:

$$G_s = \frac{(1-\mu_s)}{2LA_oI_sS_z} \qquad\qquad\qquad \text{[Eq. 3]}$$

$$G_t = \rho\left[(1.13-0.16\mu_t)\nu_s\right]^2 \qquad\qquad \text{[Eq. 4]}$$

where

G_t and G_s are the shear moduli of the concrete and the subbase, respectively

μ_t and μ_s are the Poisson ratios for the concrete and the subbase, respectively

ν_s is the surface wave velocity

L is the length of the concrete slab

S_z is the shape factor

I_s is a constant

A_o is the static flexibility of the slab (at $f = 0$).

Test Procedures

To allow for comparison, each NDE method was applied on all 47 test locations. To conduct the UPV measurements, an ultrasonic test system (Figure 3) equipped with two transducers, with a resonance frequency of 54 KHz, was used. Since this method had never been applied to testing of in-place concrete pavements, an "extended" surface transmission procedure was devised. This procedure involved making (manually) a series of UPV measurements along the longitudinal centerline of each test location (see Figure 4). First, with the transmitter fixed at the left edge of the area and the receiver at a distance (d) of 0.30 m away, the transit time (t) for the ultrasonic pulse to travel from the transmitter to the receiver was measured and recorded. Then, the measurement was repeated three times; each time the receiver was moved away from the transmitter along the centerline by 0.30 m. (Such measurements were later repeated at all test locations, with the spacing between the two transducers starting at 50 mm, then increasing by increments of 50 mm after each measurement.) For sites 2, 6, and 7, where fine longitudinal cracks were present in the concrete slabs, an additional series of measurements was made whereby the two transducers were aligned along a transverse line, i.e., perpendicular to the longitudinal centerline.

If the entire portion of the concrete slab traversed by the transducers in a test location is free of damage, it is expected that a plot of the results of the series of t versus d measurements will yield a linear relationship, allowing for slight variations arising from the natural
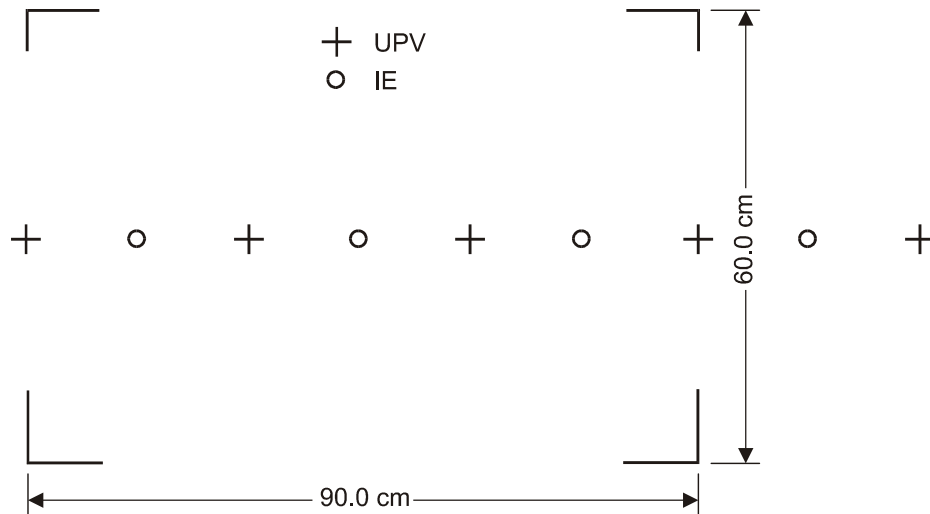
Figure 4. Points for placement of transducers used for surface UPV measurements and IE tests at each test location.
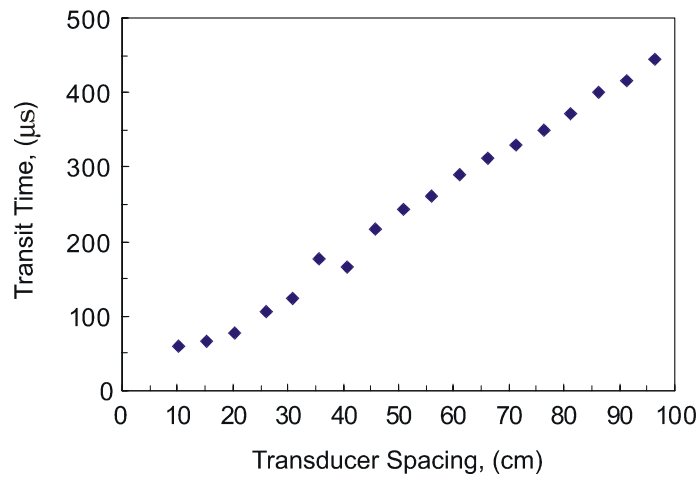
Figure 5. Plots of *t* versus *d* obtained from surface measurements of UPV made at test location 1-7.

heterogeneity in the concrete (Figure 5). The presence of a crack or other defect in the concrete may result in a significant deviation from linearity in the plot, as illustrated in Figure 6.

A field system (Figure 7) was used to conduct an IE test at each test location. The system consisted of a hand-held impactor/transducer unit, a computer-based data acquisition system, and a software system. The impactor/transducer unit housed six spherical steel impactors (of varied weights) and a sensitive displacement transducer, all properly configured for contact with the surface of the structure being tested. Because of the finite limit of the area probed by the unit, no more than approximately 30 cm around the impactor/transducer assembly, four IE measurements were made along the same longitudinal centerline at each test location (Figure 4). The software system allowed for controlling of the test parameters and the acquisition, storage, analysis, and

7
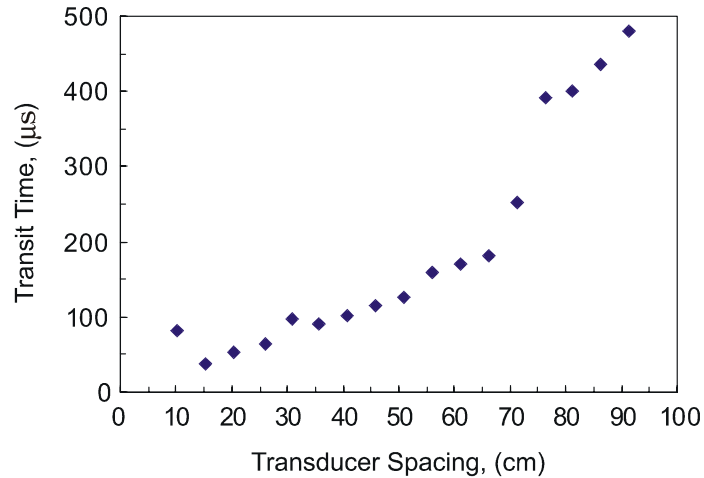
Figure 6. Plots of *t* versus d obtained from surface measurements of UPV made at test location 1-3.
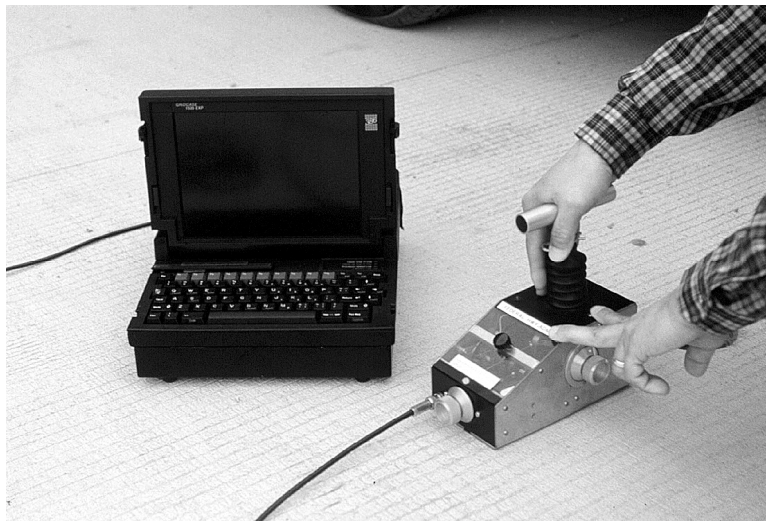
Figure 7. Field IE system, with its computer-based data acquisition system and hand-held impactor/ transducer unit.

display of the data.[5] Analysis of test data included calculating the amplitude spectrum of the reflection waveform, computing the normalized spectrum, and evaluating and classifying the normalized spectrum with a neural network. These tasks required user inputs such as the compression wave speed (v_c) and the thickness of the concrete (*d*) at each test point, which is not available and not practical to obtain.

Testing of each test location with the SPA was conducted by its developers from the University of Texas, at El Paso. This system, as shown and illustrated in Figures 8 and 9, is designed as a small trailer equipped with two pneumatic hammers and six transducers (four accelerometers and two geophones). After being towed to each test location, the trailer was positioned so that the hammers and transducers would be aligned parallel with and approximately
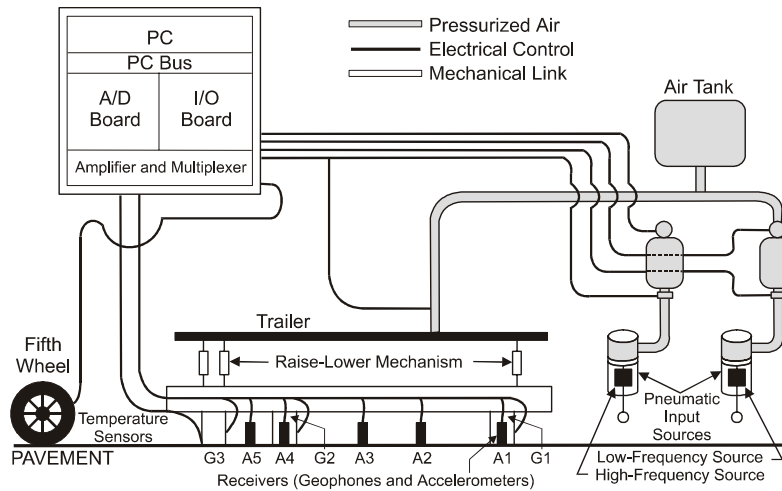
Figure 8. Schematic of SPA components.

Figure 9. Trailer-mounted SPA, equipped with two pneumatic hammers and several transducers, positioned over test location.

15 cm beyond the centerline of each test location (Figure 10) when they were mechanically lowered to make contact with the pavement surface. Then, the hammers struck the pavement several times, each time producing vibrations in the pavement that were picked up by the transducers. In response, the transducers produced electrical signals that were relayed to a computer onboard the towing vehicle. The computer then analyzed the signals and generated a report describing the pavement condition, thickness, stiffness, presence of any defects, etc.

Photographs of each test location were taken with a 35-mm camera. From these photographs, the number, total length, and approximate orientation of cracks were estimated to provide a visual evaluation of the condition of the pavement surface. In addition, at least one

LFS Low-Frequency Source
HFS High-Frequency Source
G1, G2 Geophones
A1, A2, A3, A4 Accelerometers
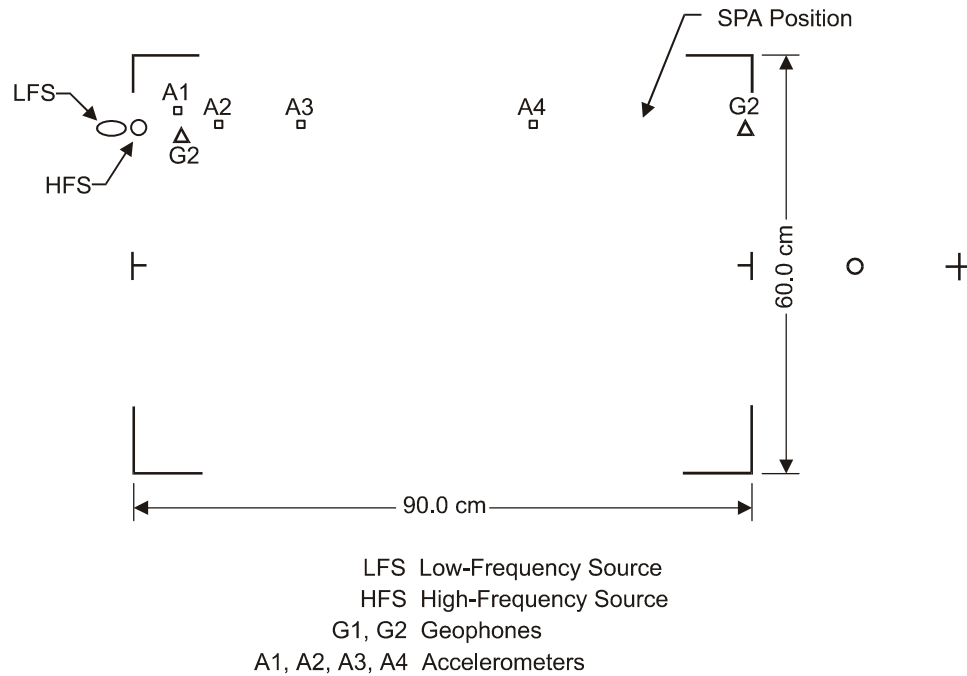
Figure 10. Typical placement of impactors and transducers of SPA at each test location.

core was extracted from each location. The physical condition of the cores was assessed by visual examination; in addition, selected cores were petrographically examined.

Cores selected for petrographic examination were cut to provide a slab with surfaces parallel with the core axis. One surface was finely lapped to provide a smooth surface for microscopic examination. The primary examination was performed at a magnification of 50X with a stereomicroscope. The surface area scanned for each specimen ranged from 45 to 92 cm^2, with an average of 68 cm^2. Approximately 1,425 fields (1.5 x 2.0 mm) distributed across the surface of the specimen were examined. The concrete component at the center point of each field (paste, aggregate, air voids) was identified. In addition, each field was scanned for features associated with concrete distress (Table 2), and the number of each feature observed was tallied.[6]

Table 2. Features Used to Develop Petrographic Damage Rating

Distress Feature	ASR Rating	ASR Weighting Factor	Crack Rating
Aggregate cracks	X	2	
Aggregate cracks with gel	X	4	
Debonded aggregate	X	0.5	
Rimmed aggregate	X	4	
Corroded aggregate	X	4	
Voids filled or lined with gel	X	0.25	
Paste cracks	X	4	X
Paste cracks with gel	X	6	

Source: Lane, D.S., *Alkali-Silica Reactivity in Virginia*, VTRC 94-R17, Virginia Transportation Research Council, Charlottesville, 1994.

10

The tallied counts of distress features were used to compute a damage rating for each core in a manner similar to that described by Grattan-Bellew.[7] Two ratings were developed for each specimen. The first considered the features noted in Table 2 multiplied by a factor (also noted in Table 2) weighted according to the association of the feature with actual damage. The weighted features were then summed, and the total was divided by the area scanned to arrive at the damage rating. Because it was known from previous surveys[7] that some pavement sections included in this study were affected by ASR, the damage rating focused on features associated with ASR.

To avoid overemphasis of ASR, a second rating, based solely on the number of observed paste cracks summed and divided by the area scanned, was computed. By using only paste cracks, this rating focuses on observable damage and thus avoided features that, although associated with a distress mechanism, may be benign in the context of physical concrete condition.

The test procedure described facilitates a direct comparison among the three NDE methods with regard to their ability to detect the distress prevailing at each test location as documented by the visual and petrographic examinations. The "best" or most accurate method, then, would be the one yielding the highest correlation between occurrences of documented defects and occurrences of NDE-detected defects.

RESULTS AND DISCUSSION

Verification of the Actual Condition of the Concrete

Photographic examination, supplemented by visual examination, proved a very valuable tool for assessing the condition of the pavement at each test location. In particular, the resulting photographs made it practical to quantify the distress in the pavement by determining the total length of different types of cracks at each test location, with minimum visits to the locations. In fact, as a result of the experience gained with photographic examination of concrete pavement in this investigation, another research effort was conducted at the Virginia Transportation Research Council to assess the feasibility of developing and implementing an automated pavement distress survey system incorporating digital image processing.[8]

After a preliminary examination of some of the results, it was considered beneficial to divide the six test sections in two groups according to the types of distress each section showed (see Table 1). Accordingly, test sections 1, 3, and 5, which had transverse cracks of various severity across the pavements such as those exemplified in Figure 1, and possibly concrete delaminations, were grouped together. The remaining test sections 2, 6, and 7, which showed the "wet" streaks of various densities on the pavement surfaces (Figure 2) and, occasionally, a transverse crack in some locations, were placed in another group.

As Table 3 indicates, the predominant type of distress observed visually in test sections 1, 3, and 5 were transverse cracks. Examination of the cores extracted from these test sections indicated that many of these transverse cracks were full depth, i.e., extending from the top to the

Table 3. Surface Cracks

Test Location	Transverse n	Transverse Length (m)	Longitudinal n	Longitudinal Length (m)	All Types n	All Types Length (m)
1-1	3	1.15	0	0	3	1.15
1-2	2	1.02	0	0	2	1.02
1-3	1	0.55	0	0	1	0.55
1-4	2	0.90	0	0	2	0.90
1-5	0	0.00	0	0	0	0.00
1-6	2	0.90	0	0	2	0.90
1-7	0	0.00	0	0	0	0.00
1-8	1	0.61	0	0	1	0.61
Total	11	5.13	0	0	11	5.13
3-1	0	0.00	0	0	0	0.00
3-2	1	0.30	0	0	1	0.30
3-3	0	0.00	0	0	0	0.00
3-4	1	0.24	0	0	1	0.24
3-5	1	0.58	0	0	1	0.58
3-6	1	0.60	0	0	1	0.60
Total	4	1.72	0	0	4	1.72
5-1	4	1.25	0	0.00	4	1.25
5-2	4	2.40	0	0.00	4	2.40
5-3	0	0.00	0	0.00	0	0.00
5-4	0	0.00	1	0.16	1	0.16
5-5	0	0.00	1	0.20	1	0.20
5-6	2	1.20	0	0.00	2	1.20
5-7	2	1.20	0	0.00	2	1.20
5-8	0	0.00	0	0.00	0	0.00
Total	12	6.05	2	0.36	14	6.41
2-1	1	0.90	20	3.88	21	4.78
2-2	0	0.00	2	0.27	2	0.27
2-3	1	0.60	19	2.97	20	3.57
2-4	1	0.60	7	1.26	8	1.86
2-5	0	0.00	0	0.00	0	0.00
2-6	1	0.60	2	0.16	3	0.76
2-7	0	0.00	34	3.43	34	3.43
2-8	0	0.00	11	1.67	11	1.67
2-9	0	0.00	9	2.70	9	2.70
2-10	0	0.00	0	0.00	0	0.00
Total	4	2.7	104	16.34	108	19.04
6-1	0	0.00	0	0.00	0	0.00
6-2	1	0.62	6	0.55	7	1.17
6-3	0	0.00	9	0.75	9	0.75
6-4	0	0.00	14	2.17	14	2.17
6-5	1	0.23	12	1.25	13	1.48
6-6	1	0.60	13	0.99	14	1.59
6-7	0	0.00	0	0.00	0	0.00
6-8	1	0.60	22	2.40	23	3.00
Total	4	2.05	76	8.11	80	10.16
7-1	0	0.00	0	0.00	0	0.00
7-2	0	0.00	3	0.21	3	0.21
7-3	0	0.00	0	0.00	0	0.00
7-4	0	0.00	3	0.32	3	0.32
7-5	0	0.00	1	0.65	1	0.65
7-6	3	0.40	0	0.00	3	0.40
7-7	0	0.00	0	0.00	0	0.00
Total	3	0.4	7	1.18	10	1.58

bottom of the concrete pavement slab (see Table 4). As a quantitative way of rating the overall severity of distress in each of these test sections, the total number and total length of each type of crack observed in all test locations in each test section were determined. Ranking these three sections in the order of increasing total number and total length of transverse cracks would yield test section 3 < section 1 < section 5 (Table 3). The amount, in both number and length, of longitudinal cracks in these test sections was insignificant.

The type of distress visually observed in test sections 2, 6, and 7 was different. As Table 3 shows, the distress was mostly longitudinal cracks. The cracks appeared to have started as longitudinal streaks with a wet appearance; they then developed into fine cracks, which eventually became interconnected by short and fine transverse cracks to form map cracking (Figure 2). Ranking these test sections in the order of increasing severity of pavement distress, based on either the total number or total length of these longitudinal cracks, would yield section 7 < section 6 < section 2 (Table 3). Examination of the cores taken from the three test sections indicated that the main underlying cause of the characteristic pavement distress was ASR in the concrete, as evidenced by the presence of white silica gel around some of the aggregate particles and voids exposed in some fractured surfaces.

The ratings from the petrographic examinations for individual cores and the average for cores from each test section are presented in Table 4. As explained earlier, higher ratings mean more defects in the sampled concrete. In comparing the average ASR ratings, sections 2, 6, and 7 had higher ratings as a group than sections 1, 3, and 5, indicating the prevalence of ASR-associated features in sections 2, 6, and 7. However, in terms of average paste-crack ratings, sections 2, 5, and 6, as a group, showed more physical damage than sections 1, 3, and 7. The average paste-crack ratings, however, grouped sections 2, 5, and 6 as showing more physical damage than sections 1, 3, and 7. Section 7, which showed ample evidence of ASR but little actual physical damage to the concrete, is an example, at least at this stage, of a nondeleterious reaction. Unfortunately, it is not possible to predict whether the reaction at location 7 will remain in a benign state or begin to expand excessively with consequent damage at a later time. The damage noted in section 5, in light of the frequency and width of transverse cracks, can be attributed to excessive shrinkage of the concrete.

Surface Measurement of UPV

Among the instrumentation used in this investigation, the ultrasonic test system used to conduct this measurement was the simplest. Widely used mainly for measurement of the UPV of concrete and detection of voids in concrete, both by the direct transmission, it has been available in its present form (a transmitter, a receiver, and a control/meter unit) for at least 20 years. Therefore, for the application intended in this investigation, the aforementioned "extended" surface transmission procedure had to be conducted manually. If this procedure is found to be useful, it can be made less time-consuming by modification of the control unit to allow for incorporation of multiple receivers in the instrumentation system.

As described earlier, if the concrete in a test location is in good condition, the resulting plot of t versus d for the surface UPV measurements conducted at each test location should be linear. Figure 5, which graphically illustrates the results of surface UPV measurements at test location 1-7, shows data points that generally fall within a straight-tending line, indicating concrete in good condition. The slight deviation (→20 :sec) from the straight line in the vicinity of a 36-cm transducer separation distance is probably due to less than uniform contacts of the transducer coupling on the textured concrete surface at different test points at the location and the natural heterogeneity of the concrete. Figure 6, on the other hand, depicts a line with a more pronounced deviation from linearity and, therefore, is a clear indication of a defect in the concrete. In this example, which is for test location 1-3, the deviation from linearity, in fact, fragmentation into two lines at a separation of 0.70 to 0.80 m, corresponded to a transverse crack on the pavement at approximately 0.68 m.

Examination of the UPV results indicated that the method could sometimes facilitate the location of relatively fine transverse cracks, which in the presence of transverse cut grooves in the pavement would not be apparent visually. The UPV results for test locations 3-4, 3-5, and 3-6 serve as clear evidence of this; an examination of black and white photographs of these locations verified the presence of fine transverse cracks, which were determined to be approximately 0.1 to 0.2 mm wide in a return visit to these locations. However, there was also an instance, as in test location 5-1, wherein the plot of t versus d revealed only the presence of a relatively wide crack near the end of the location while showing no definitive indication of three finer cracks. Likewise, the plot for test location 5-2 gave no definitive indication of three cracks, two of which were wider than those in location 5-1. (The pavement grooves in test section 5 were very worn in comparison to those in sections 1 and 3.)

Table 4 presents the results of UPV measurements at each test location in terms of the nature of the individual t versus d plot and, for comparison, the actual condition of the concrete pavement as determined by various types of examination of the pavement surface and extracted cores. (Results from the other NDE methods are also presented in Table 4.) In the interpretation of UPV results for each test location, any deviation from linearity in the t versus d plot, regardless of the extent, was considered an indication of concrete distress. The distress was liberally interpreted to indicate the presence of transverse and/or longitudinal cracks, delaminations, or fractures in the concrete, etc. As to be expected, there were agreements and disagreements between the actual concrete condition and what the t versus d plots indicated. In the first cases, either the t versus d plot indicated that the concrete was normal and the concrete did not show distress, as symbolized by +/+ in Table 5, or the plot indicated distress in the concrete and the actual concrete condition was such, or -/-. In the other cases, where the two disagreed, either the plot indicated the concrete was normal and the actual concrete condition was distressed (+/-) or vice versa (-/+).

As summarized in Table 5, in 82 percent of the test locations in test sections 1, 3, and 5, the UPV results were correct or consistent with the actual condition of the concrete. In the remaining 18 percent, there was inconsistency between what the UPV results may be indicating and the actual condition of the concrete. This reasonably favorable performance of surface UPV

measurement should be viewed with tempered enthusiasm, since the distress in these test sections were relatively advanced, mostly wide and full-depth transverse cracks.

A likely better gage of the usefulness the method for early detection of pavement problems would be test sections 2, 6, and 7, since the distress in these sections was mostly in the form of relatively subtle and fine longitudinal cracks. For these test sections, the UPV results were consistent with the actual condition of the concrete in only 68 percent of the test locations. However, three of the locations (6-1, 7-4, and 7-7) (see Table 4) whose UPV results were inconsistent with the condition of the concrete had either dense wet spots or streaks on the pavement surfaces. In this and the following comparisons involving the other NDE methods, these symptoms were not considered indicators of distress in the concrete. However, as mentioned earlier, it is likely that such symptoms are precursors of longitudinal cracks that characterized many locations in this group of test sections. If this is correct and these three test locations are considered distressed already, then the total number of locations showing UPV results being consistent with actual concrete condition would increase to 80 percent instead. This would not only be more in agreement with the statistics for the first group of test sections but, as the following discussion would reveal, also nearly identical with the statistics for the IE method (Table 5).

Impact-Echo Method

The instrumentation hardware design for the field system used for conducting this test was perhaps the most sophisticated among the systems involved in this investigation. However, its software, which was at its first-generation stage, is wanting, in particular, the neural network portion. An unpublished investigation by two of the present investigators found that this neural network could give a wrong indication of the presence of a delamination or void in the concrete if the required compression wave speed (v_c) and the thickness of the concrete (d) inputs were inaccurate.[9] Therefore, in this investigation, the investigators did not rely on the neural network but on first-hand examination of the recorded waveform and the calculated amplitude/frequency and normalized depth spectra to assess the condition of the concrete at each test location.

The IE test result for test point 2-2-1 in test location 2-2, as illustrated in Figure 11, can be considered. The time-domain waveform, shown at the top, represents a series of relatively healthy and repetitive stress wave reflections from the bottom of a sturdy concrete slab. Its corresponding amplitude/frequency and normalized depth spectra were relatively "clean" too. Combined, these results indicated that the concrete at this point was free of delamination, which is a form of advanced damage in the concrete. However, since this method relies on the disruption of stress wave propagation arising from the presence of distinct discontinuities within the concrete to assess the condition of the concrete, it often cannot detect microscopic cracks resulting from ASR. A case in point is that petrographic examinations of cores from this test location indicated that microscopic ASR-induced cracks were already present. In many cases of concrete affected by ASR, the reaction product, a viscous gel, can occupy cracks within the concrete, providing a medium with transmission properties fairly similar to those of normal concrete, thus masking the presence of discontinuities related to ASR difficult to discern.
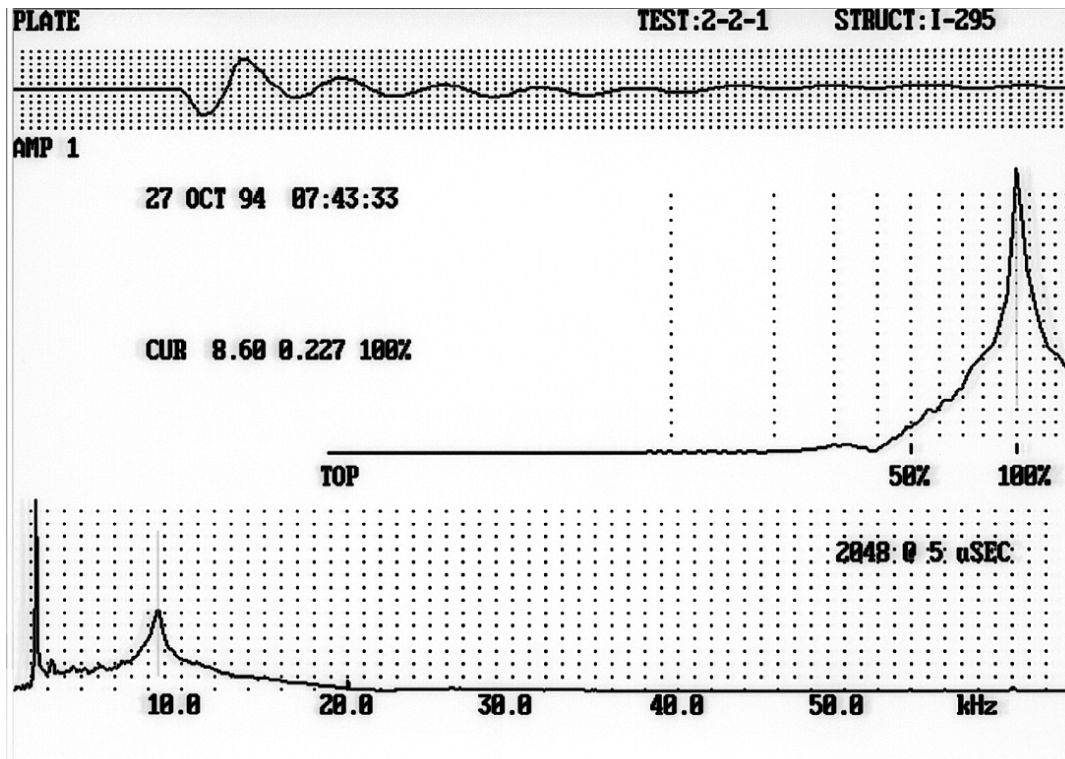
Figure 11. IE results of test obtained with field system from test location 2-2-1 showing sound concrete. The top is the surface displacement time-domain waveform; the middle is its normalized depth spectrum; the bottom is the amplitude/frequency spectrum resulting from fast-Fournier transform analysis of the displacement waveform. The 8.60-KHz peak in the amplitude spectrum corresponds to the resonance frequency *(f)* of the reflection from the bottom of the slab.

Figure 12 illustrates the IE results for test location 2-1, which had extensive macroscopic damage on the pavement and core surfaces. In contrast to Figure 11, these results lack the well-defined reflection from the bottom of the slab and the cleaned spectra that characterize macroscopically sound concrete. In this location, the concrete damage had progressed to a stage where the irregular cracks became material discontinuities that scatter the stress waves and prevent strong reflections. Figures 11 and 12 illustrate how IE may be used to evaluate the integrity of a concrete member, but they also indicate that the results can be misleading for concrete in the early stages of ASR distress.

Table 4 shows the IE test results for each test location, and Table 5 shows how these results compared with the actual condition of the concrete. For clarification, the term "flaws" is used typically by the developers of the method to describe delaminations, fractures, and sizeable voids in the concrete being tested. As to be expected, there were agreements and disagreements between what the IE tests indicated and the actual condition of the pavements. Collectively, IE appeared to have performed equally well in both groups of test sections, providing correct indications of the pavement condition in 82 percent of the test locations in test sections 1, 3, and 5 and in 84 percent of the test locations in sections 2, 6, and 7 (Table 5). These can be considered encouraging results for the IE method.

18
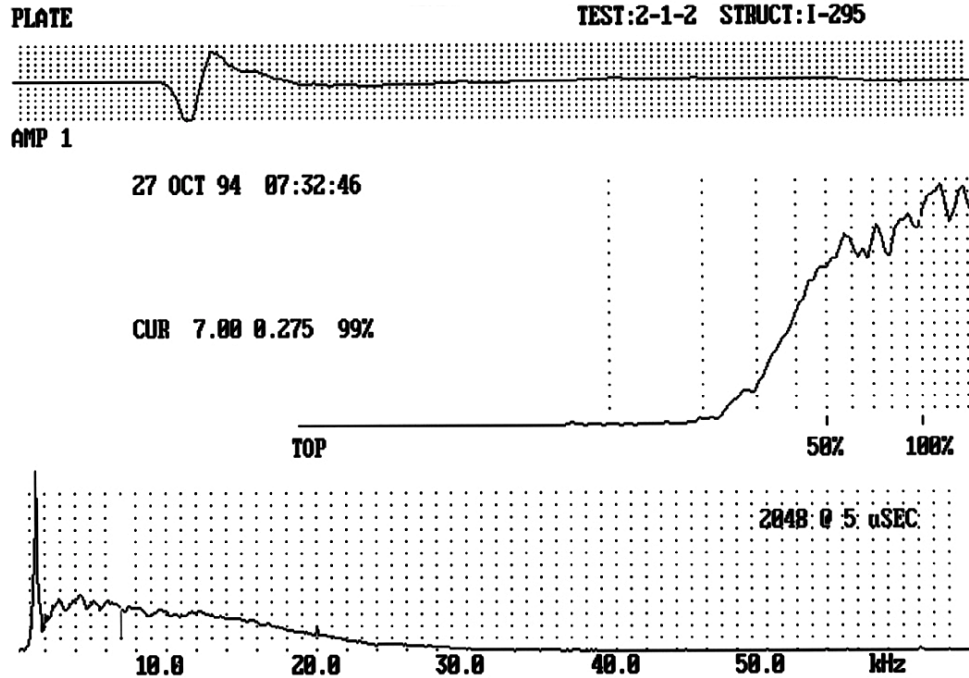
Figure 12. IE results for test location 2-1-2, which had map cracking on the surface of the concrete. Notice the differences between the displacement waveform and the depth spectra shown here and those in Figure 11, which were obtained from a location with relatively sound concrete.

Seismic Pavement Analyzer

Since it incorporates different stress wave techniques, the SPA was the most complex and comprehensive of all the systems tested. The results of the SPA tests are presented in Table 6. The comparison of the actual thickness of the concrete slab and that determined by the SPA is shown in Table 7.

As explained earlier, properties such as compression wave speed and shear wave speed are useful indicators of the relative quality of the concrete slab, and the subgrade modulus is a useful indicator of the quality of the subgrade layer. In general, the greater the values of these parameters, the better the material. The damping ratio is an indicator of the degree of resistance to movement by a concrete slab. A slab that is in good contact with the subgrade or contains a water-saturated void will show a highly damped behavior and will have a damping ratio of more than 70 percent. A slab containing an edge void will have a damping ratio on the order of 10 to 40 percent, and a slab with loss of support in the middle of the slab will have a damping ratio of 30 to 60 percent. From these results, the presence of delamination in the concrete and the condition of the pavement (the concrete itself and the subgrade) at each location were deducted, as also listed in Table 6. Unfortunately, validation of the reliability of the SPA assessment of the condition of the subgrade was beyond the scope of this investigation.

Table 6. Results of Seismic Pavement Analyzer

Test Location	Elastic Wave Speed (m/s) Compression	Shear	Thickness of Slab (mm)	Damping Ratio (%)	Subgrade Modulus (GPa)	Condition Concrete	Subgrade
1-1	3800	2500	**211**	100	1.3	average	strong
1-2	3650	2400	207	100	1.4	average	strong
1-3	3800	2200	188	100	1.4	weak	strong
1-4	3450	2400	207	100	1.1	average	average
1-5	3650	2600	207	100	0.7	average	weak
1-6	3650	2500	207	100	1.0	average	average
1-7	3450	2500	204	100	0.4	average	weak
1-8	3650	2600	207	100	1.1	average	average
Avg.	3640	2460	205	100	1.1		
3-1	3300	2600	207	100	0.9	weak	average
3-2	3550	2600	211	100	1.3	weak	strong
3-3	3550	2800	211	100	1.2	average	average
3-4	3500	2600	211	100	1.2	weak	average
3-5	3700	2500	207	100	1.1	average	average
3-6	3650	3100	202	100	0.8	average	average
Avg.	3540	2700	208	100	1.1		
5-1	2700	2200	207	100	0.6	weak	weak
5-2	3050	2400	213	100	0.3	weak	weak
5-3	3700	2700	207	100	0.5	strong	weak
5-4	3100	- -	- -	100	0.3	weak	weak
5-5	3800	2800	200	100	0.8	average	average
5-6	3500	2400	207	97	0.9	weak	average
5-7	3350	2700	211	100	0.5	weak	average
5-8	3350	2700	207	100	0.6	weak	weak
Avg.	3320	2560	207	100	0.6		
2-1	2500	2200	207	100	0.6	weak	weak
2-2	3200	2500	207	59	0.8	weak	average
2-3	2850	2500	207	37	1.0	weak	average
2-4	3350	2500	207	39	0.9	weak	average
2-5	3300	2600	204	42	1.0	weak	average
2-6	3450	2700	207	71	1.2	average	average
2-7	3450	2400	211	100	0.5	average	weak
2-8	3550	2300	213	43	0.9	weak	average
2-9	3700	2400	207	48	0.9	average	average
2-10	3350	2500	202	67	1.1	weak	average
Avg.	3270	2460	207	61	0.9		
6-1	3700	2500	- -	100	0.5	average	weak
6-2	3350	2500	213	100	0.6	weak	weak
6-3	3350	2500	207	100	0.6	weak	weak
6-4	3700	2600	179	100	0.2	average	weak
6-5	3500	2300	181	90	1.7	average	strong
6-6	3700	2600	207	- -	- -	average	- -
6-7	3400	2700	198	100	0.8	average	average
6-8	3350	2600	207	100	1.7	weak	strong
Avg.	3510	2540	199	99	0.9		

(continues)

20

| Test | Elastic Wave Speed (m/s) | | Thickness of | Damping | Subgrade | Condition | |
Location	Compression	Shear	Slab (mm)	Ratio (%)	Modulus (GPa)	Concrete	Subgrade
7-1	3700	2600	- -	100	0.8	average	average
7-2	3700	2600	200	46	1.1	average	average
7-3	3650	2700	194	78	1.1	average	average
7-4	3500	2500	198	78	1.6	weak	weak
7-5	3700	2600	141	57	2.4	average	average (?)
7-6	3400	2500	143	82	2.5	weak	weak (?)
7-7	3700	2700	190	84	2.6	average	average (?)
Avg.	3620	2600	178	75	1.7		

It is difficult to gage how well the SPA detected delaminations. At many test locations, only one core was taken, which could not necessarily be extracted directly over the area typically tested by the SPA, i.e., the upper half of each location (Figure 10). Thus, some of the cores could have easily missed some relatively small or early delaminations. The cores taken at seven locations verified the presence of delamination indicated by the SPA results, including incipient or early delaminations. However, one may assume that some of the distress interpreted by the SPA as delaminations may actually be surface cracks on the concrete as described in Tables 3 and 4. Even with a liberal interpretation of the SPA results, the system provided results that were consistent with the actual condition of the concrete at only 38 percent of the locations in test sections 1, 3, and 5 and at 74 percent of the locations in test sections 2, 6, and 7 (Table 5). It is uncertain why this system, which also incorporated the IE method, did not do as well as the field IE system in locating all types of distress in the concrete. Perhaps a combination of the design of the equipment (such as impactor, receiver, their orientation or placement, etc.) and the customized software used to interpret the reflected waveforms was the reason. The large difference between the results for the two groups of test sections is likely due to the difference in the types of cracks present and the manner in which various transducers were aligned in the SPA system (see Figure 10).

The accuracy of the SPA interpretation of the condition of the concrete is also difficult to assess. As shown in Table 8, the SPA rated the condition of the concrete at each location as weak, average, or strong. It is difficult to understand how the concrete condition at a test location such as 1-1 was rated by the SPA to be average in spite of three relatively wide and probably full-depth cracks. It may be more meaningful to consider the condition of concrete in terms of a group of locations or a section of pavement instead of individual locations. Accordingly, when the percentage of locations rated by the SPA as having weak concrete in each test section is plotted against the average petrographic ASR rating (Table 4) for the section, some interesting correlations emerged, especially when the six test sections were divided into two groups according to the predominant signs of distress on the pavement surface (Figure 13). For the group of test sections 1, 3, and 5, the correlation coefficient was 0.98; for test sections 2, 6, and 7, the correlation coefficient was 0.99.

Such a strong correlation may mean that the SPA could be used to survey a long stretch of pavement for indications of the relative condition of different sections of the pavement. Further, the relatively high degree of correlation between weak concrete and high ASR ratings in

Table 7. Comparison of Actual Thickness of Concrete Slab and That Determined by SPA

Test Location	Thickness of Concrete (mm)		Error (mm)	Average Error (mm)
	Actual	**SPA**		
1-1	209	211	2	-4
1-2	205	207	2	
1-4	211	207	-4	
1-5	212	207	-5	
1-6	213	207	-6	
1-7	210	204	-6	
1-8	216	207	-9	
3-1	195	207	12	6
3-2	200	211	11	
3-3	215	211	-4	
3-4	195	211	16	
3-5	204	207	3	
3-6	205	202	-3	
5-1	211	207	-4	-6
5-2	225	213	-12	
5-3	215	207	-8	
5-5	220	200	-20	
5-6	215	207	-8	
5-7	210	211	1	
5-8	200	207	7	
2-2	200	207	7	1
2-3	200	207	7	
2-4	195	207	12	
2-5	220	204	-16	
2-6	210	207	-3	
2-7	207	211	4	
2-8	212	213	1	
2-9	215	207	-8	
6-2	208	213	5	-7
6-6	215	207	-8	
6-7	215	198	-17	
6-8	215	207	-8	
7-2	205	200	-5	-43
7-3	208	194	-14	
7-4	207	198	-9	
7-5	250	141	-109	
7-6	225	143	-82	
7-7	230	190	-40	
		Average (mm)	-8	
		Std. Dev. (mm)	23	

the test sections where early stage ASR was present may indicate that use of the SPA can predict ASR long before cracks become apparent on the surface. As Table 6 shows, use of the SPA was
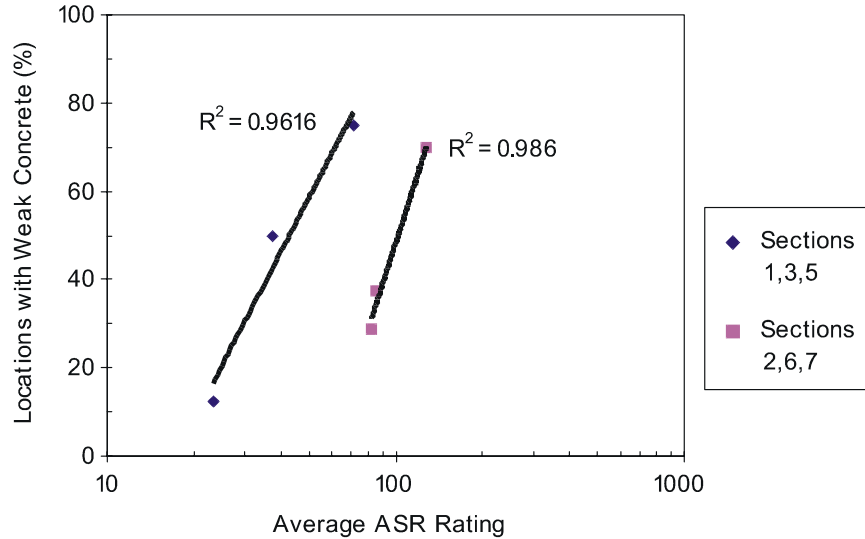
Figure 13. Correlation between average petrographic ASR rating and percentage of test locations with weak concrete in each test section as assessed by SPA. Transverse cracks and longitudinal cracks were the predominant distress in sections 1, 3, and 5 and sections 2, 6, and 7, respectively.

the only NDE technique tested that could measure such properties as subgrade modulus and damping ratio, which relate to the condition of the subgrade. Unfortunately, there is no other independent method with which to validate these SPA results.

Another type of information provided by the SPA through use of the incorporated IE technique was the thickness of the concrete slab at each location (Table 6). Table 7 compares these SPA results with the actual thickness of the concrete slab as determined from extracted cores. The only large (>20 mm) discrepancies between slab thickness measured from cores and that indicated by the SPA occurred in Section 7, where 7-5, 7-6, and 7-7 yielded discrepancies of ←109, ←82, and ←40 mm, respectively. The SPA interpreted delaminations at 7-5 and 7-6 (Table 4) suggesting a flaw at these locations significant enough to cause the strong reflection recorded. These were the only test locations where an SPA-indicated delamination corresponded to a strong reflection from the middle of the slab. IE results (Table 4) indicated that the condition of the concrete at these locations varied from uncertain to flaws likely. Further investigation into the individual IE frequency spectra recorded at the individual test points in these locations revealed the presence of a resonance frequency of approximately 40 KHz, of an intensity ranging from weak to strong, in many of these spectra. Assuming a compression velocity of 3500 to 4000 m/s, which is typical for many concretes encountered, this resonance frequency corresponded to a reflection between 4.3 and 5.4 cm from the surface. This may contribute to the SPA's extremely low estimates of the slab thickness at these locations. Delaminations were not noted from the cores taken at these locations, but as mentioned earlier, the core locations were not exactly coincident with the test points measured by the SPA at many locations.

Summary

It is possible to use either the IE method or the surface UPV method over a period of time to monitor the deterioration rate and, by extrapolation, the future condition of a pavement. However, for application in inspection of pavements, the hardware for both instrumentation systems should be developed to provide for mobility and some degree of automation. Such development would include at least enlarging the pavement area that each system can effectively probe at each pavement location, perhaps by multiplying the number of sets of transmitters and receivers; providing for a control system that automatically records or acquires the readings from all receivers; and providing for system mobility. Although the IE field system already has a software system that could serve as the basis for further development, the UPV system does not. All such developments would require considerable investment of funds and time.

In contrast, the SPA, which incorporated some aspects of these two methods, has already benefited from such development. In addition, it will likely be the only mobile NDE system in the near future that has the unique capability to provide information for the condition of both the concrete and the subgrade layer. In fact, there are ongoing efforts to improve and refine this system by its developers at the University of Texas, El Paso and to validate the system by the Federal Highway Administration.[10]

Although pavement inspection by photographic imaging does not probe the concrete as the three NDE methods/systems investigated, it is a very valuable tool for capturing the existing surface condition of any concrete pavement and pavement surface features, such as the wet streaks on some of the test sections, that may be precursors of cracks in the pavements. If used over a period of time on a pavement, photographic imaging could be a valuable tool for determining the deterioration rate of a pavement, especially if the imaging process can be digitized so that the data may be analyzed quantitatively. Even though developing software that would allow digital analysis of cracks or other subtle forms of distress would be a formidable task, the payoff would be considerable enough to warrant the effort.

CONCLUSIONS

- *Photographic inspection offers a valuable method for assessing the condition of pavements.* It is likely to be applicable also for predicting even the future condition of a pavement, especially one that is susceptible to ASR attacks, for which the visible wet streaks on the pavement surface may be indicators of upcoming distress.

- *Of the three NDE methods investigated, the IE method and the surface measurement of UPV yield the best overall results in indicating existing macroscopic cracks in a concrete pavement.* As such, it is possible to use either method to predict the future condition of a pavement by extrapolation from data collected over a period of time.

- *Even though the SPA provides information that neither the surface measurement of UPV nor the IE method yields, this investigation was not able to verify the reliability of the information.*

- *The SPA provides information that can be used to derive an assessment of the overall condition of each test section that is strongly related to the ASR rating of the section as determined by petrographic examination. This correlation may serve as the basis to predict the future condition of concrete pavements, especially those known to be susceptible to ASR attacks. The inspection system, however, could be improved.*

RECOMMENDATIONS

- *Closely monitor the development and validation of the SPA for possible future implementation.* Extra attention should be aimed at the validation efforts regarding the particular limitations discussed in this report.

- *Verify the correlation between the SPA ratings of the overall condition of pavement sections and petrographic ASR ratings of concrete.*

- *Explore the application of high-speed digital imaging of pavement surfaces as part of an integrated pavement survey system for both project and network levels.*

REFERENCES

1. Whitehurst, E.A. Evaluation of Concrete Properties from Sonic Tests. *ACI Monograph No. 2*. American Concrete Institute, Detroit, 1966.

2. Bungey, J.H. Ultrasonic Testing to Identify Alkali-Silica Reaction in Concrete. *British Journal of NDT*, Vol. 33, No. 5, pp. 227-231, 1991.

3. Carino, N.J., Sansalome, M., and Hsu, N.N. Flaw Detection in Concrete by Frequency Spectrum Analysis of Impact-Echo Waveforms. *International Advances in Nondestructive Testing*, 12th ed. Gordon & Breach Science Publishers, New York, 1986.

4. Nazarian, S., Baker, M.R., and Crain, K. *Development and Testing of a Seismic Pavement Analyzer*. Report SHRP-H-375. Strategic Highway Research Program, National Research Council, Washington, D.C., 1993.

5. Sansalone, M., and Pratt, D.G. *Theory and Operational Manual for the Impact-Echo Field System*. Cornell University, Ithaca, New York, 1992.

6. Lane, D.S. *Alkali-Silica Reactivity in Virginia.* Report No. VTRC 94-R17. Virginia Transportation Research Council, Charlottesville, 1994.

7. Grattan-Bellew, P.E. Laboratory Evaluation of Alkali-Silica Reaction in Concrete from Saunders Generating Station. *ACI Materials Journal,* Vol. 92, No. 2, pp. 126-134, 1995.

8. Howe, R., and Clemeña, G.G. *An Assessment of the Feasibility of Developing and Implementing an Automated Pavement Distress Survey System Incorporating Digital Image Processing.* Report No. VTRC 98-R1. Virginia Transportation Research Council, Charlottesville, 1997.

9. Clemeña, G.G., Lozev, M., Fowler, J., and Pritchett, M. Inspection of a Historically Significant Overlaid Bridge Deck with Impact-Echo Method. *Proceedings of Structural Materials Technology: An NDT Conference*, Atlantic City, New Jersey, February 1994.

10. Gatchalian, C. Seismic Pavement Analyzer Undergoing Field Tests in Florida. *Focu*s, Federal Highway Administration, Washington, D.C., July 1997.

Test Location	Visible Cracks (All Types) Number	Total	Visual Examination	ASR Rating	Avg.	Paste Crack/cm	Avg.	UPV	IE	SPA
1-1	3	11	transverse crack	27.78	23.22	0.45	0.39	fragmented	flaws	no concrete delaminations
1-2	2		transverse crack	27.66		0.58		fragmented	flaws	concrete delaminations
1-3	1		delaminated	20.19		0.31		fragmented	flaws likely	early delaminations
1-4	2		2 transverse cracks	17.24		0.23		fragmented	flaws	early delaminations
1-5	0		normal					fragmented	flaws likely	early delaminations
1-6	2		transverse crack					fragmented	flaws likely	concrete delaminations
1-7	0		normal					linear	flaws	early delaminations
1-8	1		normal					fragmented	flaws	no concrete delaminations
3-1	0	4	normal, voids		37.56		0.48	linear	solid	early delaminations
3-2	1		normal, voids	26.83		0.43		fragmented	flaws	early delaminations
3-3	0		normal, voids					linear	solid	early delaminations
3-4	1		normal, voids	36.87		0.63		slightly fragmented	flaws	early delaminations
3-5	1		normal, voids					slightly fragmented	flaws	early delaminations
3-6	1		shallow crack, voids	48.99		0.4		slightly fragmented	flaws possible	early delaminations
5-1	4	14	transverse crack, delamination	64.4	71.3	1.16	1.11	fragmented	flaws likely	no concrete delaminations
5-2	4		normal, voids					linear	flaws	no concrete delaminations
5-3	0		shallow crack, voids	75.11		1.44		slightly fragmented	likely solid	no concrete delaminations
5-4	1		shallow crack, voids					slightly fragmented	likely solid	weak concrete
5-5	1		shallow crack, voids					slightly fragmented	solid	early delaminations
5-6	2		transverse crack, voids					fragmented	flaws	no concrete delaminations
5-7	2		normal, voids	58.16		0.57		fragmented	flaws likely	no concrete delaminations
5-8	0		fine, shallow crack	87.51		1.25		slightly fragmented	solid	early delaminations
2-1	21	108	damaged, crack		127.94		1.86	fragmented	flaws likely	early delaminations
2-2	2		normal	177.99		2.17		linear	solid	early delaminations
2-3	20		damaged, crack					fragmented	flaws	early delaminations
2-4	8		normal					slightly fragmented	flaws likely	early delaminations
2-5	0		normal					fragmented	solid	no concrete delaminations
2-6	3		fine cracks	113.84		1.17		fragmented	flaws possible	no concrete delaminations
2-7	34		normal	152.3		3.52		slightly fragmented	flaws likely	early delaminations
2-8	11		shallow crack					linear	uncertain	concrete delaminations
2-9	9		cracks					fragmented	uncertain	early delaminations
2-10	0		normal	67.63		0.59		slightly fragmented	solid	early delaminations
6-1	0	80	normal, voids		85.76		1.12	fragmented	flaws possible	
6-2	7		normal, voids					fragmented	flaws likely	no concrete delaminations
6-3	9		delamination, vertical crack	80.1		1.61		fragmented	flaws possible	concrete delaminations
6-4	14		damaged, crack	71.55		0.76		fragmented	flaws	early delaminations
6-5	13		damaged, crack	110.16		1.26		fragmented	flaws	concrete delaminations
6-6	14		crack	63.48		1.45		fragmented	flaws	early delaminations
6-7	0		crack	74.64		0.54		fragmented	flaws likely	concrete delaminations
6-8	23		damaged, crack	114.61		1.08		fragmented	flaws	early delaminations

(continues)

Test Location	Visible Cracks (All Types) Number	Total	Visual Examination	Petrographic Evaluation ASR Rating	Avg.	Paste Crack/cm	Avg.	Nondestructive Evaluation UPV	IE	SPA
7-1	0	10	normal		82.19		0.56	fragmented	solid	
7-2	3		longitudinal crack, voids	78.42		0.52		linear	solid	no concrete delaminations
7-3	0		transverse crack, voids					slightly dev.	solid	early delaminations
7-4	3		normal, voids	57.49		0.32		fragmented	flaws likely	early delaminations
7-5	1		longitudinal crack, voids	92.18		0.71		slightly dev.	flaws likely	concrete delaminations
7-6	3		normal, voids	100.66		0.72		fragmented	flaws possible	concrete delaminations
7-7	0		longitudinal crack, voids					slightly dev.	uncertain	no concrete delaminations

Table 5. Summary of Comparison Between NDE Results and Actual Concrete Condition

NDE Results	UPV Sections 1, 3, 5		Sections 2, 6, 7		IE Sections 1, 3, 5		Sections 2, 6, 7		SPA Sections 1, 3, 5		Sections 2, 6, 7	
Agreed with Actual Concrete Condition												
Locations with +/+	3	14%	2	8%	4	18%	7	28%	0	0%	3	13%
Locations with -/-	15	68%	15	60%	14	64%	14	56%	8	38%	14	61%
Total	18	82%	17	68%	18	82%	21	84%	8	38%	17	74%
Disagreed with Actual Concrete Condition												
Locations with +/-	1	5%	1	4%	2	9%	2	8%	7	33%	2	9%
Locations with -/+	3	14%	7	28%	2	9%	2	8%	6	29%	4	17%
Total	4	18%	8	32%	4	18%	4	16%	13	62%	6	26%

15